Received: 10 July 2025 | Accepted: 26 October 2025

DOI: 10.1111/jpy.70116

RESEARCH ARTICLE

When chemistry meets taxonomy: Studying glycolipidic chemomarkers in pelagic *Sargassum* spp. (Phaeophyceae) using molecular networking

Charlotte Nirma[1] | **Valérie Stiger-Pouvreau**[1] | **Marceau Levasseur**[2] | **David Touboul**[2,3] | **Solène Connan**[1] | **Sylvain Petek**[1]

[1]Univ Brest, IRD, CNRS, Ifremer, LEMAR, IUEM, Plouzané, France

[2]CNRS, Institut de Chimie Des Substances Naturelles (ICSN), UPR 2301, Université Paris-Saclay, Avenue de la Terrasse, Gif-sur-Yvette, France

[3]Laboratoire de Chimie Moléculaire (LCM), CNRS UMR 9168, École Polytechnique, Institut Polytechnique de Paris, Route de Saclay, CEDEX, Palaiseau, France

Correspondence
Charlotte Nirma, Univ Brest, IRD, CNRS, Ifremer, LEMAR, IUEM, Plouzané F-29280, France.
Email: charlotte.nirma@univ-ubs.fr

Funding information
Centre National de la Recherche Scientifique, Grant/Award Number: 80|Prime program; Agence Nationale de la Recherche, Grant/Award Number: ANR-19-SARG-0004 and ANR-19-SARG-0008

Editor: C. Amsler

Abstract

To chemically differentiate the three pelagic *Sargassum* morphotypes co-occurring in floating rafts and drifting across the Atlantic Ocean before stranding on West African, Caribbean, and Atlantic Mexican coastlines, we conducted an investigation of their metabolomic profiles. Hydroethanolic extracts from open-sea raft specimens were analyzed using liquid chromatography–tandem mass spectrometry (LC–MS^2), and the resulting spectra were processed through feature-based molecular networking with MetGem software. Several glycolipids were putatively identified through spectral matching and manual annotation, predominantly associated with *S. natans* var. *wingei*, *S. natans* var. *natans*, and *S. fluitans* var. *fluitans*. These findings were corroborated by statistical analyses of ^{1}H NMR spectral fingerprints. This study represents a chemotaxonomic assessment of pelagic *Sargassum* utilizing molecular networking, demonstrating its efficient utility for putative chemomarker identification. We further discuss the taxonomic status of the three varieties in light of our chemical data, along with observed physiological distinctions among the morphotypes.

KEYWORDS
chemomarkers, glycolipids, molecular network, *Sargassum*

INTRODUCTION

Pelagic *Sargassum* species (Sargassaceae, Phaeophyceae) are brown macroalgae living in the open sea without any benthic attachment phase and without sexual reproduction (Stiger-Pouvreau et al., 2023). Their presence in the open sea, in the form of floating rafts of different sizes (Ody et al., 2019), constitutes a complex habitat that shelters a rich and diverse biodiversity (Huffard et al., 2014; Michotey et al., 2020; van Tussenbroek et al., 2024). Initially, these algae were observed in the original Sargasso Sea; however, since

Abbreviations: ^{1}H NMR, proton nuclear magnetic resonance; ADAP, Automated Data Analysis Pipeline; Da, Dalton; DDA, Data-Dependent Acquisition; DGDG, digalactosyldiacylglyceride; GASB, Great Atlantic *Sargassum* Belt; GNPS, Global Natural Product Social Molecular Networking; HR-MAS NMR, high-resolution magic angle spinning nuclear magnetic resonance; ISDB, In Silico DataBase; LC–MS^2, liquid chromatography coupled to tandem mass spectrometry; LPC, lysophosphatidylcholine; LPE, lysophosphatidylethanolamine; MGDG, monogalactosyldiacylglycerides; MN, molecular network; PCA, principal component analysis; PLS-DA, Partial Least Squares Discriminant Analysis; RCO, acylium ion; SQDG, sulphoquinovosyldiacylglycerides; t-SNE, t-distributed Stochastic Neighbor Embedding; VIP, variable importance in projection.

2011, new developments have been observed in the north of Brazil and in the Gulf of Mexico, leading to a massive increase in the biomass of the algae and its expansion into the tropical North Atlantic Ocean and to the creation of new Sargasso seas, notably the Great Atlantic *Sargassum* Belt (GASB; Gower et al., 2013; Wang et al., 2019). The result is a proliferation of rafts drifting with the winds and currents. But the consequences of this proliferation are not limited to the open sea. As they approach the coast, the rafts strand and the algae are degraded by bacteria, producing hydrogen sulfide and causing serious health problems for local populations (de Széchy et al., 2012; Resiere et al., 2020; Smetacek & Zingone, 2013). These mass strandings, mainly on the coasts of the Caribbean islands, the Atlantic Mexican coastline, and West Africa, are causing social and economic damage. The ecological impact is difficult to quantify, but these groundings have catastrophic consequences for benthic fauna and flora (van Tussenbroek et al., 2017).

Sargassum species in the Sargasso Sea have been studied for decades, but recent research has focused on understanding this new proliferation phenomenon and the origin of the species involved. The study of drifting rafts has revealed the presence of three varieties corresponding to three morphotypes belonging to two pelagic species: *Sargassum natans* var. *wingei* (morphotype SN8), *S. natans* var. *natans* (morphotype SN1), and *S. fluitans* var. *fluitans* (morphotype SF1; Schell et al., 2015; Dibner et al., 2022; Siuda et al., 2024). The three morphotypes can be distinguished morphologically (Kergosien et al., 2024; Siuda et al., 2024), and under the same environmental conditions, they exhibit different physiology such as growth rate (Changeux et al., 2023; Magaña-Gallegos, García-Sánchez, et al., 2023; Magaña-Gallegos, Villegas-Muñoz, et al., 2023). However, it is still difficult to differentiate them at the molecular level (Amaral-Zettler et al., 2017; González-Nieto et al., 2020; Sissini et al., 2017; Siuda et al., 2024). A recent morphometric and chemical analysis distinguished the three *Sargassum* varieties by examining fatty acid ratios but without identifying a chemomarker to distinguish the two varieties of *S. natans* (Kergosien et al., 2024). Thus, the isolation of a chemomarker specific to one of the varieties of *S. natans* could lead us to conduct a taxonomic revision within the floating varieties of pelagic *Sargassum*. Various analytical techniques can be used for this purpose, including liquid chromatography (LC) or gas chromatography (GC), mass spectrometry (MS), and nuclear magnetic resonance spectroscopy (NMR). These techniques have made it possible, used separately or in combination, to identify metabolomic variations in different species of the same genus. A study of four species of the brown macroalgal genus *Lobophora* using LC–MS, GC–MS, and NMR spectroscopy identified polyunsaturated alcohols as chemomarkers (Gaubert et al., 2019). In the Sargassaceae family, studies have been carried out to identify chemomarkers enabling morphological classification to be revised. In the *Cystoseira*/*Gongolaria*/*Ericaria* complex, a combined LC–MS^n and HR-MAS NMR analysis was used to differentiate five species encountered in Brittany, France (Jégou et al., 2010, 2012). Interestingly, cyclized merditerpenes were isolated as chemomarkers of *Gongolaria nodicaulis*, which were not identified in the other specimens of the complex. Always within the Sargassaceae family, turbinaric acid, a lipidic chemomarker, had also been identified in *Turbinaria conoides*, and never in *T. ornata*, by coupling GC–MS and HR-MAS NMR techniques and using a large geographical sampling of both species (Le Lann et al., 2008, 2014). Chemotaxonomic studies can also highlight spatiotemporal variations in the algal metabolome, as in the case of the brown Sargassaceae macroalga *Bifurcaria bifurcata* (Le Lann et al., 2014), which presented diterpene variations with hydrodynamical conditions and seasons, and also in *S. muticum*, which presented different metabolomic fingerprints in relation to a latitudinal gradient, from Portugal to Norway (Tanniou et al., 2015). Metabolomic analysis of pelagic *Sargassum* has been used for the discrimination of benthic species by GC–MS and infrared spectroscopy (Rosado-Espinosa et al., 2020), ^{1}H NMR, and HR-MAS NMR analysis, to differentiate between pelagic morphotypes (Hernández-Bolio et al., 2021; Kergosien et al., 2024). However, to date, no chemomarker has been identified in these pelagic *Sargassum* varieties.

The present study is based on the assumption that the three morphotypes living together in rafts have different chemical signatures and can be differentiated using metabolomic fingerprints. Pelagic *Sargassum* samples were collected in Guadeloupe, a region impacted by massive strandings. Samples were then analyzed by LC–MS^2; tandem mass spectra were used to generate feature-based molecular networks (MNs). Molecular networks allow spectral similarities to be represented as a 2-D graph. If two molecules have similar fragmentation spectra (including neutral loss and diagnostic fragments), we can hypothesize that they have similar structures and therefore belong to the same molecular family. It is therefore possible to identify clusters of structurally similar molecules.

For over a decade, the use of molecular networks for the study and in silico annotation of MS^2 spectra has represented a major advance in the analysis of complex mixtures, enabling large data sets to be visualized on a spectral similarity map. As fragmentation spectra provide structural information, it is possible to compare experimental spectra with spectral databases to identify compounds or at least their analogs. Numerous libraries are available and can be queried for network annotation: Global Natural Product Social Molecular Networking (GNPS; Wang et al., 2016) or In Silico Database (ISDB; Allard et al., 2016) or those available on MS-Dial (Tsugawa et al., 2020). Molecular networks

are, therefore, powerful tools for dereplicating and identifying the algal metabolome.

This organization and visualization technique has already been used to study the metabolome of the brown macroalgae *Taonia atomaria* (Carriot et al., 2021) and *Fucus vesiculosus* (Buedenbender et al., 2020). Both studies used the GNPS online platform, offering the scientific community the possibility of generating feature-based molecular networks from their LC-MS^2 data and visualizing them via Cytoscape (Wang et al., 2016). However, the MNs generated by GNPS lose an important piece of information, namely the link (or degree of chemical proximity) between clusters. For this reason, MetGem software (https://metgem.github.io/) has been developed for calculating and visualizing feature-based molecular networks by integrating a t-distributed Stochastic Neighbor Embedding (t-SNE) representation keeping information about the cluster distances. This visualization provides new keys for annotating MNs (Olivon et al., 2018).

Using MetGem is straightforward, follows the same workflow as analysis via GNPS, can be used on a local session, and allows optimized data preprocessing on MZMine (Olivon et al., 2017). MetGem's interface also provides a graphical representation of the data set, eliminating the need for an additional visualization tool such as Cytoscape.

Beyond the differentiation of morphotypes, the metabolomic study of these varieties offers fertile ground for exploring the morphological adaptations of these algae to their environment and thus possibly understanding their origins. Characterizing the metabolic profiles of algae in different ecological and experimental contexts will provide new insights into their adaptation to environmental conditions as well as into their biotechnological potential for industrial, health, and environmental applications.

MATERIALS AND METHODS

Sampling

Samples of each variety or morphotype, *Sargassum natans* var. *wingei* (SN8), *S. natans* var. *natans* (SN1), and *S. fluitans* var. *fluitans* (SF1), were collected in situ from floating rafts along the Guadeloupe coastline on June 10, 2021 (off the coast of Petit Havre Beach, 16°11.061'N; 61°25.523'W). After collection, the epiphytes were removed and the samples were briefly rinsed with tap water. The samples were then freeze-dried for 72 h and ground into powder. Samples were stored at the Laboratory of Environmental Marine Sciences (LEMAR) laboratory as herbarium specimens under the reference numbers 21.G.L.S1.1, 21.G.L.S1.2, and 21.G.L.S1.3 for SN8 samples; 21.G.L.S2.1, 21.G.L.S2.2, and 21.G.L.S2.3 for SN1 samples; and 21.G.L.S3.1, 21.G.L.S3.2, and 21.G.L.S3.3 for SF1 samples.

Metabolites extraction

Depending on the subsequent analyses, two types of extraction were carried out: one on 15 mg of algal dry powder (LC–MS^2 analysis) and another on 500 mg using two different solvents (^{1}H NMR analysis).

Then, for the LC-MS^2 analysis, 15 mg of freeze-dried powder (from 21.G.L.S1.1, 21.G.L.S2.1, and 21.G.L.S3.1 samples) were placed in Eppendorf tubes with 1.5 mL of a 50:50 H_2O:ethyl alcohol (EtOH) mixture under agitation at 40°C for 2 h. After centrifugation (6797 *g* for 10 min), the supernatant was retained, and this operation was repeated two times. The supernatants were combined and evaporated to dryness to obtain the *Sargassum* hydroethanolic crude extract. Extraction was carried out under the same conditions for all three morphotypes.

In order to identify the discriminating compounds observed thanks to the molecular networks, extraction was oriented toward apolar compounds. For this, two different extracts were prepared using two solvents: acetone and dichloromethane. Both extractions were performed using 500 mg freeze-dried powder of .1, .2, and .3 biological replicate samples for each morphotype, in 10 mL of solvent. After three successive extractions and centrifugations, the supernatants of each replicate were combined and evaporated to dryness to give two apolar extracts, acetone and dichloromethane. Each crude extract was made in triplicate and analyzed using ^{1}H NMR spectroscopy.

Reverse-phase liquid chromatography-electrospray ionization in positive mode-high-resolution tandem mass spectrometry

The chromatographic system used was a UHPLC 1260 Infinity II (Agilent Technologies, Waldbronn, Germany). The system was coupled to a QToF 6546 tandem mass spectrometer (Agilent Technologies, Waldbronn, Germany). Chromatographic separation was performed on an Accucore RP-MS column (100 × 2.1 mm, 2.6 μm, Thermo Scientific, Les Ulis, France) with the mobile phase consisting of (A) H_2O:formic acid (99.9:0.1; v/v) and (B) acetonitrile. The column oven temperature was set at 45°C. Compounds were eluted at a flow rate of 0.4 mL · min^{-1} with a gradient from 5% B to 100% in 20 min, then 100% B for 6 min, and equilibration with 5% B for 2 min. The injection volume was set at 5 μL for all analyses. Mass spectra were acquired in positive ion mode. The electrospray source was configured with the following parameters: gas temperature: 325°C, drying gas flow rate: 10 L · min^{-1}, nebulizer pressure: 30 psi, sheath gas temperature: 350°C, sheath gas flow rate: 10 L · min^{-1}, capillary voltage: 3500 V, nozzle

voltage: 500 V, fragmentor voltage: 130 V, skimmer voltage: 45 V, and Octopole 1 RF voltage: 750 V. The use of a calibration solution, containing two internal reference masses (purine, $C_5H_4N_4$, *m/z* 121.0509, and HP-921 hexakis—1H,1H,3H-tetrafluoropentoxy—phosphazene, $C_{18}H_{18}O_6N_3P_3F_{24}$, *m/z* 922.0098), routinely resulted in mass accuracy below 3 ppm. Data-dependent MS^2 events were acquired for the five most intense ions detected by full-scan MS, in the *m/z* 100–1700 range, above an absolute threshold of 1000 counts. Selected precursor ions were fragmented with a fixed collision energy of 20 eV and with an isolation window of 1.3 amu. The mass range of the precursor and fragment ions was set to *m/z* 100–1700 and 50–1700, respectively.

Molecular network processing

The MS^2 data files were converted from Agilent Technologies data format to mzXML format using MSConvert software from the ProteoWizard package. Data were then preprocessed using MZMine v. 2.53 (Pluskal et al., 2010) based on the methodology previously described by Olivon et al. (2017). Mass detection was performed by maintaining the noise level at 1000 for MS level 1 and at 5 for MS level 2. Automated Data Analysis Pipeline (ADAP) chromatogram builder (Myers et al., 2017) was used with a minimum scan group size of 3, a group intensity threshold of 1000, a highest minimum intensity of 1000, and an *m/z* tolerance of 0.008 or 20 ppm. Deconvolution was performed using the ADAP wavelet algorithm with a median *m/z* center calculation, an *m/z* range for MS^2 of 0.05 Da, a retention time (RT) range for MS^2 of 0.5 min, an S/N threshold of 10, a minimum feature height of 1000, a coefficient of 10 for a peak duration range between 0.01 and 1.5 min, and a RT wavelet range of 0.00–0.04 min. Isotopes were grouped using the isotopic peaks grouper algorithm with an *m/z* tolerance of 0.008 or 20 ppm, a RT tolerance of 0.2 min, and a maximum charge of 2, using the most intense mode for the representative isotope. Peak alignment was performed using the join aligner module with an *m/z* tolerance of 0.008 or 20 ppm, a weight for *m/z* of 80%, a RT tolerance of 0.1 min, and a weight for RT of 20%. The MGF files of spectral data and their corresponding CSV metadata files were exported using the Export for GNPS option.

MetGem parameters

Cosine scores and molecular networks were calculated using MetGem 1.3.6 software (Olivon et al., 2018). The MS^2 spectra were window-filtered by selecting only the six highest peaks in the ±50 Da window across the entire spectrum. The data were filtered by removing all peaks in the ±17 Da range around the precursor *m/z*. The *m/z* tolerance windows used to find matching peaks were set at 0.04, and cosine scores were considered for spectra sharing at least two matching peaks. The minimum cosine score to link two nodes was set at 0.60. For standard searches in MetGem's associated databases (GNPS, MS-Dial, and ISDB), the parameters were as follows: *m/z* tolerance = 0.2 Th (Thomson); minimum matched peaks = 2; minimum intensity = 0%; parent *m/z* tolerance = 17 Th; minimum cosine score = 0.60. For the search for analogs, the same parameters were used and the *m/z* tolerance for the precursor ion was set at 100.

Proton nuclear magnetic resonance analysis

Dry acetone and dichloromethane crude extracts were dissolved in 0.6 mL deuterated chloroform ($CDCl_3$). The ^1H NMR spectra were recorded on a Bruker Avance 400 MHz spectrometer in the UBO Shared Service facility (Brest, France). Acquisitions were recorded using the standard pulse sequences available in Bruker software (Bruker, France), with 32 scans. Spectra were processed using MestReNova software.

Statistical analysis

The ^1H NMR spectra were processed with MestReNova software. Spectra were automatically Fourier-transformed, and baselines were corrected using Whittaker's smoother correction, then normalized. MestreNova's features were used to bin the spectra with a width of 0.001 ppm. The bin ranged from 0 to 10 ppm. The spectra were normalized to the largest peak. After stacking the spectra, the data set was exported in .txt format as a matrix and processed in a spreadsheet. The regions of δ 7.18–7.32 ppm corresponding to the $CDCl_3$ signal, as well as the region of δ 5.25–5.35 ppm corresponding to traces of residual dichloromethane solvent (only for dichloromethane extracts), were removed to eliminate the effects of these abundant signals in the multivariate analysis. The resulting data matrices were submitted to MetaboAnalyst 6.0 software for statistical analysis. Principal component analyses (PCAs) and partial least squares discriminant analysis (PLS-DA) were performed with sum normalization and without scaling data on the two matrices obtained for acetone and dichloromethane extracts.

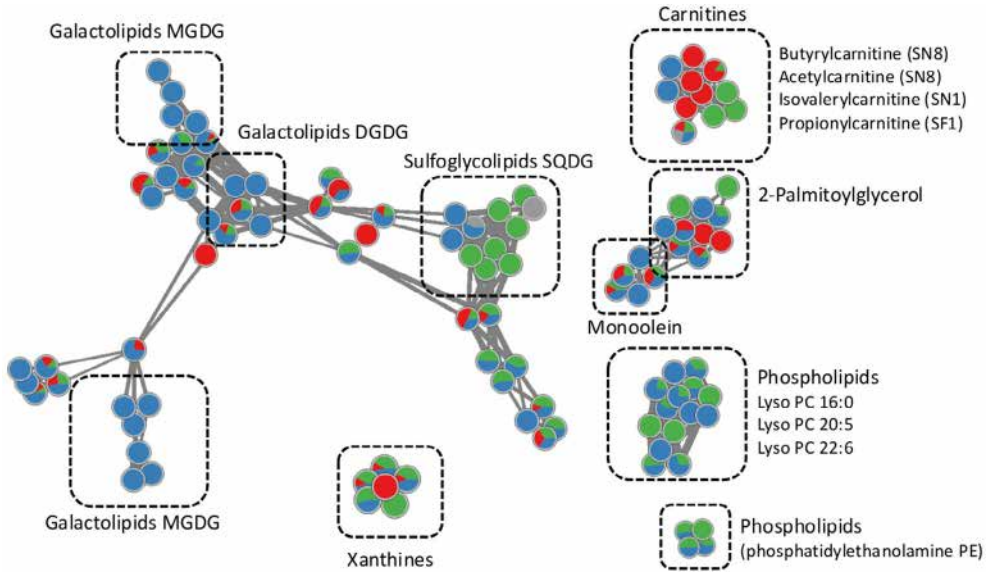

FIGURE 1 Molecular network of annotated metabolites from the H_2O/EtOH extract of SN8, SN1, and SF1 by LC-HRMS^2 analysis (107 nodes belonging to six clusters represented). Cluster annotation was performed using MetGem databases. The pie charts in the nodes represent abundance, and the colors correspond to the three morphotypes or analytical blank (red: SN8, blue: SN1, green: SF1, and gray: Analytical blank).

RESULTS

Analysis of hydroethanolic extracts

To identify chemomarkers capable of discriminating among the three morphotypes of pelagic *Sargassum*, hydroalcoholic extracts were analyzed using reverse-phase liquid chromatography coupled with electrospray ionization high-resolution tandem mass spectrometry (RPLC-ESI-HRMS^2) in Data-Dependent Acquisition (DDA) mode. The resulting spectra were preprocessed using MZMine 2.53. Data-Dependent Acquisition mode enabled the fragmentation of precursor ions in a complex sample and providing structural information about the molecules. Structurally related molecules tend to exhibit similar MS^2 fragmentation patterns, allowing for the construction of feature-based molecular networks through spectral alignment and comparison.

Feature-based molecular networks obtained using MetGem software revealed 2128 nodes, each corresponding to an individual molecular feature (precursor ion with its MS^2 spectrum at a defined retention time). Among these, 1347 nodes were grouped into 56 clusters, while 781 remained as singletons. Cluster organization was calculated according to the spectral similarity of the fragmentation patterns, using a cosine score between 0 (no similarity) and 1 (perfect match). These molecular networks were generated using a cosine score of 0.60. Nodes were color-coded with the SN8 morphotype in red, SN1 in blue, and SF1 in green. An entirely blue node corresponded to a molecule identified only in the SN1 extract. Pie charts represented the proportion of a molecule in the different morphotypes/varieties. The experimental spectra were then compared with those in the public databases available on MetGem. When the experimental spectra matched the libraries, the nodes were annotated. For the annotations shown in Figure 1, the GNPS (Wang et al., 2016), MS-Dial (Tsugawa et al., 2020), and ISDB (Allard et al., 2016) databases were queried.

Among the compounds annotated through spectral similarity within the databases, the majority were lipid compounds (phospholipids, galactolipids, etc.). Comparison with the databases also revealed the presence of carnitines and xanthines (data not processed in this study). A closer look at lipids revealed that they were predominantly identified in SN1 (blue nodes) and SF1 (green nodes). Since the seaweeds were collected at the same time and in the same station, and the extracts from each morphotype were prepared and analyzed under the same conditions, we can hypothesize that these lipid compounds are less diverse in SN8. This molecular family would then be discriminating in the differentiation of the pelagic *Sargassum* varieties. This hypothesis was supported by previous results obtained by Kergosien et al. (2024) identifying fatty acid ratios as a possibility/ability to discriminate morphotypes.

We, therefore, focused on discriminating molecules, namely glycolipids. Three types of glycolipids were putatively identified, and most of them are synthesized by algae: monogalactosyldiacylglycerides (MGDGs), digalactosyldiacylglycerides (DGDGs), and sulphoquinovosyldiacylglycerides (SQDGs). Table 1 lists the precursor and fragment ions of MGDG, DGDG, and SQDG annotated in this study by comparison of their fragmentation spectra with spectral databases and by annotation propagation and manual dereplication of the spectra (manual annotation in molecular networking refers to

TABLE 1 Major ions and their putative annotations of compounds detected in pelagic *Sargassum* hydroethanolic extracts.

Class	*n*	Precursor ion $[M+NH_4]^+ \pm SD^a$ (*m/z*)	RT ± *SD*[a] (min)	MS/MS (*m/z*)	Adduct formula	Theoretical *m/z*	Δ *m/z* ppm	Annotated fatty acids	Occurrence in varieties			Potential chemomarker in varieties
									SN8	SN1	SF1	
MGDG	1	740.5301	21.2	561; 543; 313; 305	$C_{41}H_{74}NO_{10}$	740.5313	1.6	16:0/16:4			x	SF1
	2	742.5454	21.8	563; 545; 313; 307	$C_{41}H_{76}NO_{10}$	742.5469	2.0	16:0/16:3		x		SN1
	3	744.5606	22.0	547; 337; 313; 309	$C_{41}H_{78}NO_{10}$	744.5626	2.6	16:0/16:2		x		SN1
	4	770.5961	22.1	591; 573; 335; 313	$C_{43}H_{80}NO_{10}$	770.5782	–23.2	16:0/18:3		x		SN1
	5	772.5917 ± 0.0013	22.7 ± 0.0	575; 337; 313	$C_{43}H_{82}NO_{10}$	772.5939	2.8	16:0/18:2	x	x	x	No
	6	790.5622	20.6	611; 593; 335; 333	$C_{45}H_{76}NO_{10}$	790.5469	–19.3	18:3/18:4		x		SN1
	7	792.5609	21.0	613; 585; 335	$C_{45}H_{78}NO_{10}$	792.5626	2.1	18:3/18:3		x		SN1
DGDG	8	902.5859	20.0	561; 543; 313; 305	$C_{47}H_{84}NO_{15}$	902.5841	–2.0	16:0/16:4		x		SN1
	9	904.597	20.2	563; 545; 527; 313; 307	$C_{47}H_{86}NO_{15}$	904.5998	3.0	16:0/16:3		x		SN1
	10	930.6124	20.4	589; 571; 335; 311	$C_{49}H_{88}NO_{15}$	930.6154	3.2	16:1/18:3	x			SN8
	11	932.6293 ± 0 0.0004	21.2 ± 0.0	573; 335; 313	$C_{49}H_{90}NO_{15}$	932.6311	1.9	16:0/18:3		x	x	SN8
SQDG	12	810.5391	25.4	549; 537; 313; 311	$C_{41}H_{80}NO_{12}S$	810.5401	1.3	16:0/16:1		x		SN1
	13	812.5578	25.4	551; 539; 465; 331; 313	$C_{41}H_{82}NO_{12}S$	812.5558	–2.5	16:0/16:0			x	SF1
	14	834.5379	25.2	591; 573; 465; 335; 313	$C_{43}H_{80}NO_{12}S$	834.5401	2.7	16:0/18:3			x	SF1
	15	838.5708	25.4	577; 339; 313	$C_{43}H_{84}NO_{12}S$	838.5714	0.7	16:0/18:1			x	SF1

[a]For ions detected in more than one morphotype, the precursor ion *m/z* and the retention time are presented as mean ± standard deviation. Retention time's standard deviation for these compounds was smaller than 0.05 min.

the identification of fragment ions in MS^2 spectra by assigning them to specific structural features or neutral losses, based on chemical knowledge and literature, which complements automated database matching by validating or refining candidate molecular identities). These ions were identified as $[M+NH_4]^+$ in the positive ion mode. The t-SNE projection of the MetGem software (Figure S1) highlighted the presence of other molecules structurally close to glycolipids identified in other clusters spread across the network. However, comparison with the databases did not allow us to annotate these compounds. Nevertheless, the proximity of the t-SNEs suggests spectral similarity, facilitating manual annotation of these compounds. All MS^2 spectra of annotated compounds (1–15) have been featured in Figures S2–S16, and spectral matching information has been presented in Table S1.

These putative annotations were refined by studying the detailed fragmentation of each species. The HRMS spectra exhibited signal ion peaks characteristic of these compounds, confirming the presence of these molecular classes (Da Costa et al., 2016; Körber et al., 2023; Lopes et al., 2019; Zianni et al., 2013). An example of a fragmentation study for each glycolipid class is shown in Figure 2. For MGDG, the MS^2 spectrum of compound 2 (*m/z* 742.5454, $C_{41}H_{76}NO_{10}$, Δ*m/z* 2 ppm, Figure 2a) showed an ion at *m/z* 545.4545 assigned as $[M+NH_4\text{-}197]^+$, resulting from the combined loss of NH_3 (–17 Da) and a hexose (–180 Da) due to cleavage of the sugar bond near the hemiacetal oxygen bond with proton transfer to give a diacylglycerol structure. Neutral losses also provide information on chain length and number of unsaturations. Thus, among the fatty acids identified, C16 chains without unsaturation (–256.24 Da) are frequently observed. The composition of fatty acyl chains can be deduced by the presence of product ions corresponding to each fatty acyl group in the form of an acylium plus 74 ion (RCO + 74). The 74 amu adduct corresponds to the glycerol-derived fragment $C_3H_6O_2$, which combines with the fatty acyl chain acylium ion (RCO^+) during fragmentation of glycoglycerolipids. In the case of the MGDG spectrum, RCO ions were detected at *m/z* 307.2262 and 313.2739 corresponding to C16:3 and C16:0, respectively.

Similarly, for DGDG, the MS^2 spectrum of the compound 9 (*m/z* 904.5970, $C_{47}H_{86}NO_{15}$, Δ*m/z* 3 ppm, Figure 2b) exhibited the loss of the carbohydrate fraction (–[180 + 162] Da) combined with the loss of NH_3 (–17 Da), leading to the formation of the product ion at *m/z* 545.4587, indicated as $[M+NH_4\text{-}359]^+$. These neutral losses confirmed the molecular family. The ion at *m/z* 563.4702 corresponded to the loss of the digalactosyl group. The $[RCO+74]^+$ ions were detected at *m/z* 313.2758 and 307.2284, corresponding to C16:0 and C16:3, respectively.

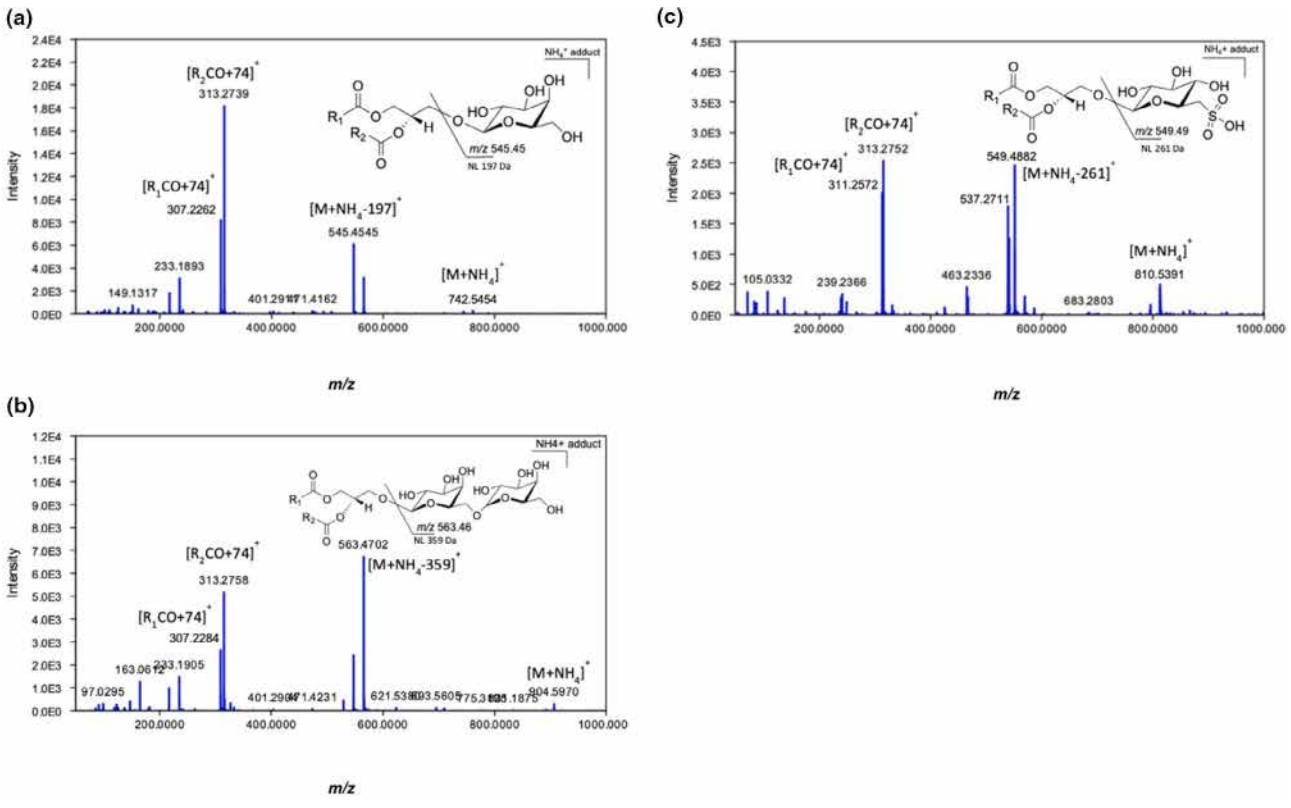

FIGURE 2 LC-MS^2 spectra of the three types of glycolipids identified by spectral comparison, and main fragmentation. (a) compound 2 $[M+NH_4]^+$ MGDG ion with *m/z* 742.5454, (b) compound 9 $[M+NH_4]^+$ DGDG ion with *m/z* 904.5970, and (c) compound 12 $[M+NH_4]^+$ SQDG ion with *m/z* 810.5391. (NL, Neutral loss).

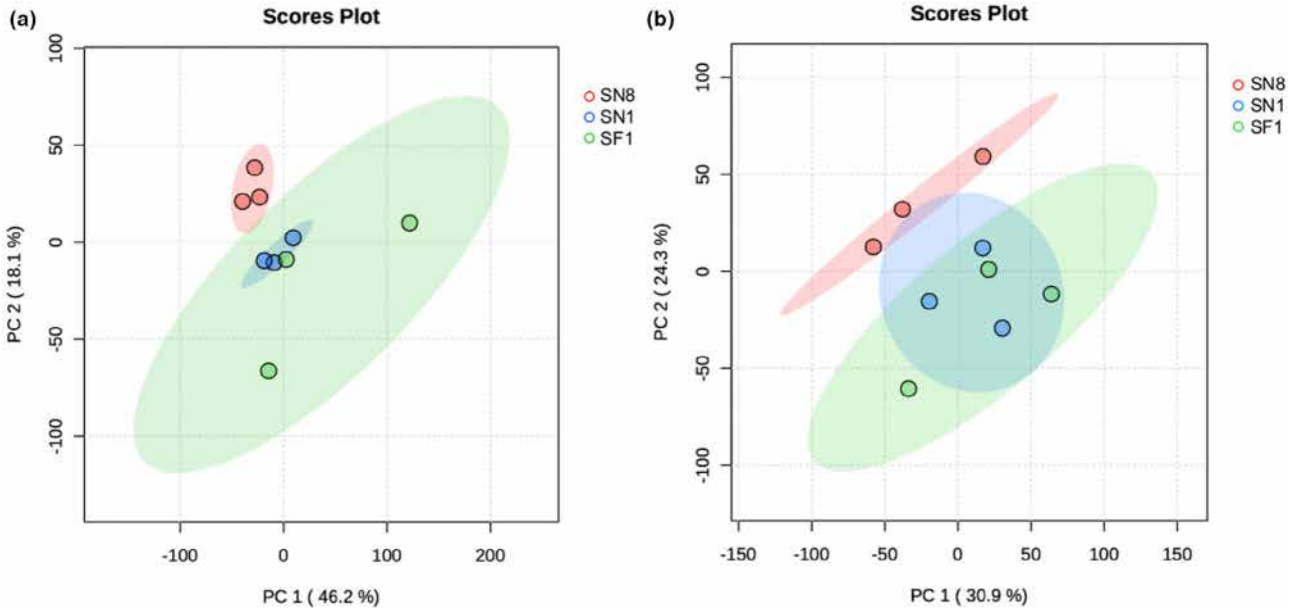

FIGURE 3 Score plot of principal component analyses of ^{1}H NMR profiles of (a) acetone and (b) dichloromethane extracts from sargassum morphotypes.

In the case of SQDGs (Figure 2c), a neutral loss of 261 Da from the $[M+NH_4]^+$ ion was observed for compound 12 at *m/z* 810.5391 ($C_{41}H_{80}NO_{12}S$, Δ*m/z* 1.3 ppm) leading to the product ion at *m/z* 549.4882 corresponding to the loss of the sulfo-group and NH_3. The RCO ions of the carbon chains were then observed, visible at *m/z* 311.2572 and 313.2752, corresponding to C16:1 and C16:0 respectively.

It appeared that MGDGs and DGDGs were more represented in the SN1 morphotype, whereas SQDGs were mainly observed in the SF1 morphotype (Table 1). However, these glycerolipid classes were poorly represented (MGDG and DGDG) or even absent (SQDG) in the SN8 morphotype. Analysis of the data revealed several molecules of interest as specific chemomarkers. Their exclusive detection suggests that they can be used as distinctive markers to discriminate between varieties. In addition, several compounds were observed in two out of three varieties; this partial distribution profile also suggests that these molecules can be considered as chemomarkers of the variety in which they are absent. Thus, their absence becomes as informative as their presence, reinforcing their usefulness in chemotaxonomic approaches to discriminate between pelagic *Sargassum* varieties.

The molecular network also showed a cluster of phospholipids that were mainly represented in the SN1 and SF1 morphotypes in different quantities (Figure 1). Comparison with the database proposed compounds identified from the phospholipid class: lysophosphatidylcholine (LPC) 16:0 (*m/z* 496.357 $[M+H]^+$, $C_{24}H_{50}NO_7P$), LPC 20:5 (*m/z* 542.3232 $[M+H]^+$, $C_{28}H_{48}NO_7P$), and LPC 22:6 (*m/z* 568.3398 $[M+H]^+$, $C_{30}H_{50}NO_7P$). Another cluster identified a lysophosphatidylethanolamine (LPE) 18:1 (*m/z* 480.3087 $[M+H]^+$, $C_{23}H_{46}NO_7P$).

Preliminary results obtained from molecular networks of LC-MS^2 spectra showed that the compounds discriminating pelagic *Sargassum* morphotypes mainly belonged to the lipid class. Research was therefore focused on apolar extracts. With the aim of identifying other chemomarkers or confirming those identified by MS^2, acetone and dichloromethane extracts were made from the three *Sargassum* morphotypes to study their metabolic profiles by ^{1}H NMR technique. The ^{1}H NMR spectra obtained were aligned and split into bins using MestReNova software. The matrices obtained for the acetone and dichloromethane profiles were then analyzed in MetaboAnalyst 6.0. A PCA was performed to visualize metabolome variation as a function of morphotypes.

Analysis of acetone and dichloromethane extracts

The PCAs obtained with the ^{1}H NMR profiles of the acetone and dichloromethane extracts are presented in Figure 3. The score plot (PC1 vs. PC2), with 64.3% of the variance explained for acetone extracts (Figure 3a) and 55.2% for dichloromethane extracts (Figure 3b), divided the samples into two groups. Whatever the extraction solvent, we could clearly see that the metabolic fingerprints of the SN1 and SF1 morphotypes were grouped together on the score plot graphs. The fingerprints obtained for morphotype SN8 were isolated in another group, which certainly indicates the presence of different metabolites.

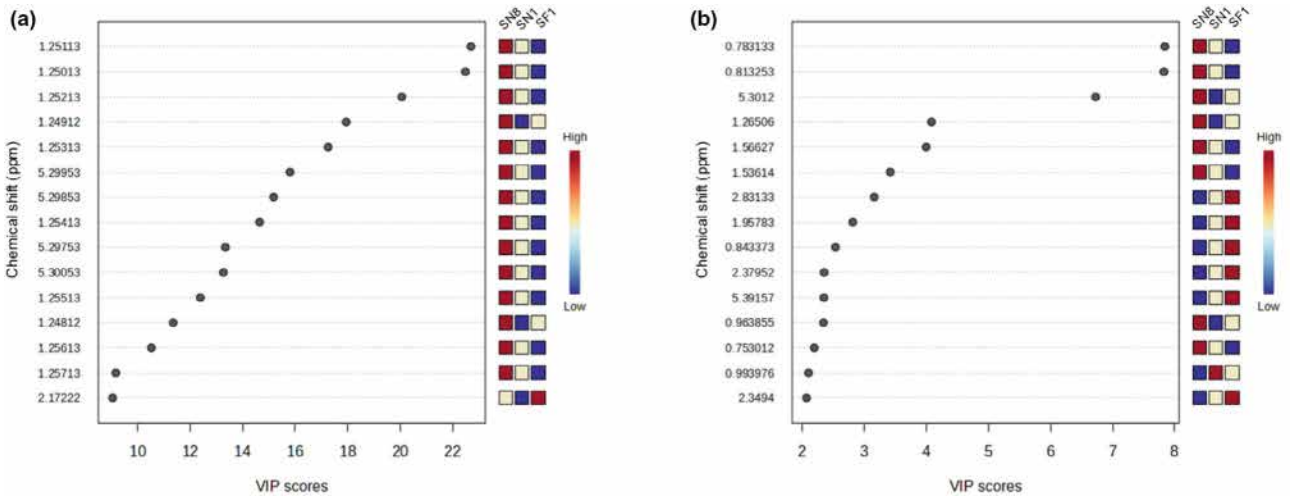

FIGURE 4 Variable importance in projection scores of partial least squares discriminant analysis of ^{1}H NMR profiles of (a) acetone and (b) dichloromethane extracts from *Sargassum* morphotypes. The colored boxes on the right indicate the relative concentrations of corresponding metabolites in each group under study.

Given the PCA results, which revealed that the samples were structured into distinct groups, a PLS-DA analysis was performed to identify the most discriminating variables (Figure S17). Analysis of the PLS-DA loading plots represents a factorial map of the variable's weights. The variables responsible for separating the groups were distributed on either side of the graph by analogy with the samples that over- or underexpress them, highlighting the discriminating variables. Variable importance in projection (VIP) values were calculated for each variable to indicate their contribution to the observed discrimination (Figure 4). In our study, these variables represented the discriminant bins or chemical shifts of possible chemomarkers between varieties. For example, for the acetone extract fingerprints (Figure 4a), the discriminant variables were signals δ 1.25 and 5.29. These signals could be representative of glycolipid compounds identified by LC-MS^2. The signal at 1.25 ppm was not incompatible with an aliphatic chain chemical shift, whereas the signal at 5.29 ppm could have been a proton of the asymmetric carbon of glycerol (regularly observed between 5.29–5.34 ppm in glycosylglycerolipids) or olefin protons carried by acyl chains, often observed in the unsaturated fatty acids (Buedenbender et al., 2020; Knaack et al., 2021; Plouguerné et al., 2010). The VIP of the dichloromethane extracts (Figure 4b) showed that the bins with the greatest influence on SN8 clustering were almost similar to those identified in the acetone extract. Among the most discriminating signals were those corresponding to chemical shifts under 1 ppm that should correspond to terminal methyl groups of the carbon chains. Signals were also present at δ 5.30–5.39 ppm (glycerol asymmetric carbon or olefinic hydrogens), 1.26 ppm (aliphatic chain), and 1.95 ppm (allylic CH_2). The signals at 2.34–2.37 ppm, which may have belonged to the alpha-methyl protons of the carbonyl group, and the signals at 1.53–1.56 ppm (beta-CH_2) were also identified. In order to certify the chemical shift assignments obtained for the NMR spectra discriminant variables, it would be necessary to perform complementary 2-D NMR HSQC spectra in order to show C-H correlations. However, the chemical shifts observed for protons seemed compatible with the identification of fatty acid chains, which may belong to glycolipids. Although different extraction protocols and analytical techniques were applied (LC-MS^2 for the hydroethanolic extracts enriched in polar lipids and ^{1}H NMR analysis for the acetone and dichloromethane extracts targeting apolar metabolites), both approaches seemed to converge on the same set of chemical markers. This apparent overlap can be explained by the amphiphilic nature of glycolipids, which are soluble in both partially polar and apolar solvents and therefore detectable in both extract types.

Statistical analysis showed that SN8 had a distinct metabolic signature, whereas SN1 and SF1 shared more similarities in their ^{1}H NMR profile. Moreover, ^{1}H NMR and MS analyses seemed to indicate that identified chemomarkers in the lipid family may be related.

DISCUSSION

The pelagic *Sargassum* varieties, responsible for mass strandings in the tropical North Atlantic Ocean, are currently classified into three morphotypes belonging to two species, *S. natans* and *S. fluitans*. Although morphological criteria can be used to differentiate these morphotypes (Kergosien et al., 2024; Siuda et al., 2024), it is important to study their molecular composition in order to identify or highlight one or more chemomarkers

that can be used to differentiate them. This study focused on the search for discriminant compounds in the metabolomic profiles of pelagic *Sargassum* extracts. Chemotaxonomic study of *Sargassum* using a molecular network approach represents a method of interest, as it enables medium-throughput analysis of metabolites. Furthermore, species discrimination can be performed without requiring prior knowledge of the genome, unlike genetic barcoding, which requires the design of specific probes.

Extracts from the three morphotypes were analyzed by LC-MS^2. This highly sensitive technique makes it possible to annotate minor compounds in the extract. The construction of molecular networks from the MS^2 spectra enabled us to quickly visualize the diversity of molecules present in the extracts studied. To generate these molecular networks, we used a spectral alignment algorithm based on MetGem software. Comparison with the spectral databases enabled us to putatively annotate compounds belonging to the glycolipid class, mainly represented in the SN1 and SF1 extracts. Seven MGDGs, four DGDGs, and four SQDGs were annotated by spectral comparison and proposed manual annotation. These compounds are present in the chloroplasts of eukaryotic algae (Hölzl & Dörmann, 2019). Monogalactosyldiacylglycerides and SQDGs are the most abundant lipids in the thylakoid membrane and play important roles in photosynthesis. These compounds are present in not only brown macroalgae (mainly in Fucales) but also in red and green algae (Plouguerné et al., 2014).

Among the 15 compounds putatively identified in this study, certain polar lipids, such as DGDG (16:1/18:3) for SN8, MGDG (16:0/16:3) for SN1, and SQDG (16:0/18:1) for SF1, stood out as exclusive and robust chemomarkers. Their unique presence in a single variety and absence in the others suggest a strong discriminatory value, essential for rapid and reliable identification. More interestingly, certain molecules shared by two varieties but absent in the third reinforced their role as indirect negative tracers. For example, the absence of DGDG (16:0/18:3) in SN8, although detected in SN1 and SF1, underlined its relevance for excluding this variety in comparative analyses.

Beyond these discriminating compounds, it is worth noting that a large fraction of metabolites overlapped across the three morphotypes. Although the present study focused primarily on exclusive or discriminant chemomarkers, shared metabolites may also carry valuable taxonomic and ecological information. They could represent conserved biochemical traits that reflect evolutionary constraints or common physiological requirements within pelagic *Sargassum*. A deeper investigation specifically targeting these overlapping compounds would be necessary to better evaluate their roles and potential significance in the chemotaxonomic interpretation.

The discriminating molecules putatively identified using feature-based molecular networks were essentially fatty acids. These results confirmed the results of a study by Kergosien et al. (2024), who reported that fatty acids constituted a family of discriminating molecules in the study of Caribbean pelagic *Sargassum* morphotypes. That study highlighted the quantification of certain compounds: palmitoleic acid (16:1n-7) for SN8, α-linoleic acid (18:3n-3) for SN1, and myristic acid (14:0) for SF1. A calculation of the ratios of those fatty acids was used to establish a dichotomous determination key for the different morphotypes (Kergosien et al., 2024).

The present study has highlighted a distinction in the metabolic profile of SN8 compared with SN1 and SF1. Although SN8 and SN1 have been described as belonging to the same species, *Sargassum natans* (Amaral-Zettler et al., 2017; Dibner et al., 2022), molecular analysis of lipidomic fingerprints appears to be more discriminating and distinguishes SN8.

This differentiation between SN8 and SN1 was already reported in a study of pelagic *Sargassum* stranded on the east coast of the Mexican Caribbean using NMR spectroscopy (Hernández-Bolio et al., 2021). In their study, the comparison of the NMR profiles of hydroethanolic extracts from the three morphotypes showed clear variation in the multivariate statistical analyses. The compounds responsible for this variation were identified as amino acids (glutamine and glutamate), myo-inositol, and trimethylamine. Although the families of molecules responsible for the variation were glycolipids in the present study on alive samples (collected in the open sea), our results confirmed that the SN8 morphotype has a different metabolic fingerprint from the two other morphotypes.

We can presume that the three pelagic morphotypes evolved together (sympatry) in *Sargassum* rafts drifting on the Atlantic Ocean, as they have been observed together in these rafts. However, we may wonder how to explain this metabolic variation in SN8. The main difference was observed in glycolipids from the thylakoids, and this could result in differences in the physiology (photosynthesis, growth) of the morphotype SN8 compared to the two other morphotypes. Indeed, SN8 is characterized by a slower growth and nutrient uptake than the two other morphotypes, as demonstrated by in situ experiments carried out in a Martinique Bay (Changeux et al., 2023) and ex situ experiments in Mexico (Magaña-Gallegos, García-Sánchez, et al., 2023; Magaña-Gallegos, Villegas-Muñoz, et al., 2023). This difference in physiology represents an adaptive strategy to nutrients, developed by SN8 but not shared by SN1 or SF1. However, in another in situ experiment carried out by the last authors (Magaña-Gallegos, García-Sánchez, et al., 2023), SN8 exhibited a higher growth rate compared to SF1, showing the physiological variations that could be observed

according to the environmental conditions (either in an enclosed bay in Martinique or near an open shore on the Mexican coastline). Finally, these physiological results have raised the question of whether SN8 and SN1 belong to the same species. With a simpler approach than genomic analysis, this study has demonstrated the applicability of a chemotaxonomic approach to pelagic *Sargassum* for discrimination based on distinctive metabolic profiles. Molecular network analysis was particularly relevant for this medium-throughput application, enabling the identification of chemomarkers, notably glycolipids. Complementary MS^2 and ^1H NMR analyses confirmed previously identified markers (fatty acid family), reinforcing the robustness and value of this strategy in studying the specific diversity of pelagic *Sargassum* species.

The chemotaxonomic approach used here involved extraction followed by LC-MS^2 analysis, which is considered rapid compared to the approach of isolating molecular markers, which requires DNA extraction and purification; PCR isolation of markers; and sequencing, which can take ~10 days. This molecular approach does not currently allow, with the markers used, a distinction between the two varieties SN8 and SN1, as shown by Amaral-Zettler et al. (2017) and Sissini et al. (2017), even if low divergence exists between both morphotypes of *Sargassum natans* (Siuda et al., 2024). In contrast, the workflow described in this study allowed the acquisition of chemical fingerprints within a much shorter time frame, while simultaneously providing functional insights into metabolite diversity. Therefore, this approach offers a valuable and time-efficient complement to traditional morphological and molecular methods.

The study of differences in morphotype profiles represents a challenge for understanding the origin, drift, and persistent development of the phenomenon of massive growth and stranding of *Sargassum* varieties along tropical Atlantic coasts.

CONCLUSIONS

This metabolomic study of pelagic *Sargassum* sought to identify one or more chemomarkers to differentiate three morphotypes. To this end, LC-MS^2 analyses of open ocean *Sargassum* extracts were carried out, and the results were analyzed using molecular networks. This study revealed the presence of glycolipids in greater quantities in the SN1 and SF1 morphotypes. To confirm these preliminary results, ^1H NMR spectra of apolar *Sargassum* extracts were analyzed, and statistical tests also revealed a clustering of SN1 and SF1 morphotypes.

This study of pelagic *Sargassum* morphotypes using molecular networks with MetGem software has shown that MetGem software is a tool of choice for identifying discriminating chemomarkers. It is now necessary to extend this study using a larger cohort of samples and to evaluate the potential of molecular networks, notably by working with other extraction solvent polarities and negative ionization. This study opens up exciting prospects for annotating the metabolome and genome of pelagic *Sargassum* species or, even, extending to the genus *Sargassum*. It also raises new questions about whether geographic variation or seasonal dynamics may drive the observed differences in lipid composition between morphotypes.

AUTHOR CONTRIBUTIONS

Charlotte Nirma: Conceptualization (equal); formal analysis (lead); investigation (lead); writing – original draft (lead); writing – review and editing (equal). **Valérie Stiger-Pouvreau:** Conceptualization (equal); funding acquisition (equal); writing – review and editing (equal). **Marceau Levasseur:** Investigation (supporting); resources (equal); writing – review and editing (equal). **David Touboul:** Investigation (supporting); resources (equal); writing – review and editing (equal). **Solène Connan:** Conceptualization (equal); funding acquisition (equal); writing – review and editing (equal). **Sylvain Petek:** Conceptualization (equal); funding acquisition (equal); writing – review and editing (equal).

ACKNOWLEDGMENTS

The authors thank the laboratories LEMAR and ICSN for their help and all the technical facilities that enabled us to carry out this work.

FUNDING INFORMATION

This work, part of the SARGASSUM ORIGINS and SAVE-C projects, was supported by grants from ANR under the call SARGASSUM Programme 2019 (Grants No. ANR-19-SARG-0004 and ANR-19-SARG-008, respectively). This work is part of C.N.'s Postdoctoral project. We acknowledge the Laboratory of Marine Sciences (LEMAR UMR 6539) set at IUEM (UBO) for their financial support. This work has received financial support from the CNRS through the 80|Prime program for the PhD of M.L.

ORCID

Charlotte Nirma https://orcid.org/0000-0002-3238-1616

REFERENCES

Allard, P. M., Péresse, T., Bisson, J., Gindro, K., Marcourt, L., Pham, V. C., Roussi, F., Litaudon, M., & Wolfender, J. L. (2016). Integration of molecular networking and in-silico MS/MS fragmentation for natural products dereplication. *Analytical Chemistry*, *88*(6), 3317–3323. https://doi.org/10.1021/acs.analchem.5b04804

Amaral-Zettler, L. A., Dragone, N. B., Schell, J., Slikas, B., Murphy, L. G., Morrall, C. E., & Zettler, E. R. (2017). Comparative

mitochondrial and chloroplast genomics of a genetically distinct form of *Sargassum* contributing to recent "golden tides" in the Western Atlantic. *Ecology and Evolution*, *7*(2), 516–525. https://doi.org/10.1002/ece3.2630

Buedenbender, L., Astone, F. A., & Tasdemir, D. (2020). Bioactive molecular networking for mapping the antimicrobial constituents of the baltic brown alga *Fucus vesiculosus*. *Marine Drugs*, *18*(6), 311. https://doi.org/10.3390/md18060311

Carriot, N., Paix, B., Greff, S., Viguier, B., Briand, J. F., & Culioli, G. (2021). Integration of LC/MS-based molecular networking and classical phytochemical approach allows in-depth annotation of the metabolome of non-model organisms - the case study of the brown seaweed *Taonia atomaria*. *Talanta*, *225*, 121925. https://doi.org/10.1016/j.talanta.2020.121925

Changeux, T., Berline, L., Podlejski, W., Guillot, T., Stiger-Pouvreau, V., Connan, S., & Thibaut, T. (2023). Variability in growth and tissue composition (CNP, natural isotopes) of the three morphotypes of holopelagic *Sargassum*. *Aquatic Botany*, *187*, 103644. https://doi.org/10.1016/j.aquabot.2023.103644

Da Costa, E., Silva, J., Mendonça, S. H., Abreu, M. H., & Domingues, M. R. (2016). Lipidomic approaches towards deciphering glycolipids from microalgae as a reservoir of bioactive lipids. *Marine Drugs*, *14*(5), 101. https://doi.org/10.3390/md14050101

de Széchy, M. T. M., Guedes, P. M., Baeta-Neves, M. H., & Oliveira, E. N. (2012). Verification of *Sargassum natans* (Linnaeus) Gaillon (Heterokontophyta: Phaeophyceae) from the Sargasso Sea off the coast of Brazil, western Atlantic Ocean. *Check List*, *8*(4), 638–641. https://doi.org/10.15560/8.4.638

Dibner, S., Martin, L., Thibaut, T., Aurelle, D., Blanfuné, A., Whittaker, K., Cooney, L., Schell, J. M., Goodwin, D. S., & Siuda, A. N. S. (2022). Consistent genetic divergence observed among pelagic *Sargassum* morphotypes in the western North Atlantic. *Marine Ecology*, *43*(1), e12691. https://doi.org/10.1111/maec.12691

Gaubert, J., Greff, S., Thomas, O. P., & Payri, C. E. (2019). Metabolomic variability of four macroalgal species of the genus *Lobophora* using diverse approaches. *Phytochemistry*, *162*, 165–172. https://doi.org/10.1016/j.phytochem.2019.03.002

González-Nieto, D., Oliveira, M. C., Núnez Resendiz, M. L., Dreckmann, K. M., Mateo-Cid, L. E., & Sentíes, A. (2020). Molecular assessment of the genus *Sargassum* (Fucales, Phaeophyceae) from the Mexican coasts of the Gulf of Mexico and Caribbean, with the description of *S. xochitlae* sp. nov. *Phytotaxa*, *461*, 254–274.

Gower, J., Young, E., & King, S. (2013). Satellite images suggest a new *Sargassum* source region in 2011. *Remote Sensing Letters*, *4*(8), 764–773. https://doi.org/10.1080/2150704X.2013.796433

Hernández-Bolio, G. I., Fagundo-Mollineda, A., Caamal-Fuentes, E. E., Robledo, D., Freile-Pelegrin, Y., & Hernández-Núñez, E. (2021). NMR metabolic profiling of *Sargassum* species under different stabilization/extraction processes. *Journal of Phycology*, *57*(2), 655–663. https://doi.org/10.1111/jpy.13117

Hölzl, G., & Dörmann, P. (2019). Chloroplast lipids and their biosynthesis. *Annual Review of Plant Biology*, *70*, 51–81. https://doi.org/10.1146/annurev-arplant-050718

Huffard, C. L., von Thun, S., Sherman, A. D., Sealey, K., & Smith, K. L. (2014). Pelagic *Sargassum* community change over a 40-year period: Temporal and spatial variability. *Marine Biology*, *161*(12), 2735–2751. https://doi.org/10.1007/s00227-014-2539-y

Jégou, C., Culioli, G., Kervarec, N., Simon, G., & Stiger-Pouvreau, V. (2010). LC/ESI-MSn and 1H HR-MAS NMR analytical methods as useful taxonomical tools within the genus *Cystoseira* C. Agardh (Fucales; Phaeophyceae). *Talanta*, *83*(2), 613–622. https://doi.org/10.1016/j.talanta.2010.10.003

Jégou, C., Culioli, G., & Stiger-Pouvreau, V. (2012). Meroditerpene from *Cystoseira nodicaulis* and its taxonomic significance. *Biochemical Systematics and Ecology*, *44*, 202–204. https://doi.org/10.1016/j.bse.2012.05.003

Kergosien, N., Helias, M., Le Grand, F., Cérantola, S., Simon, G., Nirma, C., Thibaut, T., Berline, L., Changeux, T., Blanfuné, A., Connan, S., & Stiger-Pouvreau, V. (2024). Morpho- and chemotyping of holopelagic *Sargassum* species causing massive strandings in the Caribbean region. *Phycology*, *4*(3), 340–362. https://doi.org/10.3390/phycology4030018

Knaack, W., Hölzl, G., & Gisch, N. (2021). Structural analysis of glycosylglycerolipids using NMR spectroscopy. In D. Bartels & P. Dörmann (Eds.) *Plant lipids: Methods and protocols* (pp. 249–272). Humana Press. https://doi.org/10.1007/978-1-0716-1362-7_14

Körber, T. T., Sitz, T., Abdalla, M. A., Mühling, K. H., & Rohn, S. (2023). LC-ESI-MS/MS analysis of sulfolipids and galactolipids in green and red lettuce (*Lactuca sativa* L.) as influenced by sulfur nutrition. *International Journal of Molecular Sciences*, *24*(4), 3728. https://doi.org/10.3390/ijms24043728

Le Lann, K., Kervarec, N., Payri, C. E., Deslandes, E., & Stiger-Pouvreau, V. (2008). Discrimination of allied species within the genus *Turbinaria* (Fucales, Phaeophyceae) using HRMAS NMR spectroscopy. *Talanta*, *74*(4), 1079–1083. https://doi.org/10.1016/j.talanta.2007.08.021

Le Lann, K., Kraffe, E., Kervarec, N., Cerantola, S., Payri, C. E., & Stiger-Pouvreau, V. (2014). Isolation of turbinaric acid as a chemomarker of *Turbinaria conoides* (J. Agardh) Kützing from South Pacific Islands. *Journal of Phycology*, *50*(6), 1048–1057. https://doi.org/10.1111/jpy.12235

Lopes, D., Moreira, A. S. P., Rey, F., da Costa, E., Melo, T., Maciel, E., Rego, A., Abreu, M. H., Domingues, P., Calado, R., Lillebø, A. I., & Rosário Domingues, M. (2019). Lipidomic signature of the green macroalgae *Ulva rigida* farmed in a sustainable integrated multi-trophic aquaculture. *Journal of Applied Phycology*, *31*(2), 1369–1381. https://doi.org/10.1007/s10811-018-1644-6

Magaña-Gallegos, E., García-Sánchez, M., Graham, C., Olivos-Ortiz, A., Siuda, A. N., & van Tussenbroek, B. I. (2023). Growth rates of pelagic *Sargassum* species in the Mexican Caribbean. *Aquatic Botany*, *185*, 103614.

Magaña-Gallegos, E., Villegas-Muñoz, E., Salas-Acosta, E. R., Barba-Santos, M. G., Silva, R., & van Tussenbroek, B. I. (2023). The effect of temperature on the growth of holopelagic *Sargassum* species. *Phycology*, *3*(1), 138–146.

Michotey, V., Blanfuné, A., Chevalier, C., Garel, M., Diaz, F., Berline, L., Le Grand, L., Armougom, F., Guasco, S., Ruitton, S., Changeux, T., Belloni, B., Blanchot, J., Ménard, F., & Thibaut, T. (2020). In situ observations and modelling revealed environmental factors favouring occurrence of *Vibrio* in microbiome of the pelagic *Sargassum* responsible for strandings. *Science of the Total Environment*, *748*, 141216. https://doi.org/10.1016/j.scitotenv.2020.141216

Myers, O. D., Sumner, S. J., Li, S., Barnes, S., & Du, X. (2017). One step forward for reducing false positive and false negative compound identifications from mass spectrometry metabolomics data: New algorithms for constructing extracted ion chromatograms and detecting chromatographic peaks. *Analytical Chemistry*, *89*(17), 8696–8703. https://doi.org/10.1021/acs.analchem.7b00947

Ody, A., Thibaut, T., Berline, L., Changeux, T., André, J. M., Chevalier, C., Blanfuné, A., Blanchot, J., Ruitton, S., StigerPouvreau, V., Connan, S., Grelet, J., Aurelle, D., Guéné, M., Bataille, H., Bachelier, C., Guillemain, D., Schmidt, N., Fauvelle, V., … Ménard, F. (2019). From in situ to satellite observations of pelagic *Sargassum* distribution and aggregation in the tropical North Atlantic Ocean. *PLoS ONE*, *14*(9), 2584. https://doi.org/10.1371/journal.pone.0222584

Olivon, F., Elie, N., Grelier, G., Roussi, F., Litaudon, M., & Touboul, D. (2018). MetGem software for the generation of molecular networks based on the t-SNE algorithm. *Analytical Chemistry*,

90(23), 13900–13908. https://doi.org/10.1021/acs.analchem.8b03099

Olivon, F., Grelier, G., Roussi, F., Litaudon, M., & Touboul, D. (2017). MZmine 2 data-preprocessing to enhance molecular networking reliability. *Analytical Chemistry*, *89*(15), 7836–7840. https://doi.org/10.1021/acs.analchem.7b01563

Plouguerné, E., da Gama, B. A. P., Pereira, R. C., & Barreto-Bergter, E. (2014). Glycolipids from seaweeds and their potential biotechnological applications. *Frontiers in Cellular and Infection Microbiology*, *4*, 174. https://doi.org/10.3389/fcimb.2014.00174

Plouguerné, E., Ioannou, E., Georgantea, P., Vagias, C., Roussis, V., Hellio, C., Kraffe, E., & Stiger-Pouvreau, V. (2010). Antimicrofouling activity of lipidic metabolites from the invasive brown alga *Sargassum muticum* (Yendo) Fensholt. *Marine Biotechnology*, *12*(1), 52–61. https://doi.org/10.1007/s10126-009-9199-9

Pluskal, T., Castillo, S., Villar-Briones, A., & Orešič, M. (2010). MZmine 2: Modular framework for processing, visualizing, and analyzing mass spectrometry-based molecular profile data. *BMC Bioinformatics*, *11*, 395. https://doi.org/10.1186/1471-2105-11-395

Resiere, D., Mehdaoui, H., Florentin, J., Gueye, P., Lebrun, T., Blateau, A., Viguier, J., Valentino, R., Brouste, Y., Kallel, H., Megarbane, B., Cabie, A., Banydeen, R., & Neviere, R. (2020). *Sargassum* seaweed health menace in the Caribbean: Clinical characteristics of a population exposed to hydrogen sulfide during the 2018 massive stranding. *Clinical Toxicology*, *59*(3), 215–223. https://doi.org/10.1080/15563650.2020.1789162

Rosado-Espinosa, L. A., Freile-Pelegrín, Y., Hernández-Nuñez, E., & Robledo, D. (2020). A comparative study of *Sargassum* species from the Yucatan peninsula coast: Morphological and chemical characterisation. *Phycologia*, *59*(3), 261–271. https://doi.org/10.1080/00318884.2020.1738194

Schell, J. M., Goodwin, D. S., & Siuda, A. N. S. (2015). Recent *Sargassum* inundation events in the Caribbean: Shipboard observations reveal dominance of a previously rare form. *Oceanography*, *28*(3), 8–10. https://doi.org/10.5670/oceanog.2015.70

Sissini, M. N., De Barros Barreto, M. B. B., Széchy, M. T. M., De Lucena, M. B., Oliveira, M. C., Gower, J., Liu, G., De Oliveira Bastos, E., Milstein, D., Gusmão, F., Martinelli-Filho, J. E., Alves-Lima, C., Colepicolo, P., Ameka, G., & De Graft-Johnson, K. (2017). The floating *Sargassum* (Phaeophyceae) of the South Atlantic Ocean—likely scenarios. *Phycologia*, *56*, 321–328.

Siuda, A. N. S., Blanfuné, A., Dibner, S., Verlaque, M., Boudouresque, C. F., Connan, S., Goodwin, D. S., Stiger-Pouvreau, V., Viard, F., Rousseau, F., Michotey, V., Schell, J. M., Changeaux, T., Aurelle, D., & Thibaut, T. (2024). Morphological and molecular characters differentiate common morphotypes of Atlantic holopelagic *Sargassum*. *Phycology*, *4*(2), 256–275. https://doi.org/10.3390/phycology4020014

Smetacek, V., & Zingone, A. (2013). Green and golden seaweed tides on the rise. *Nature*, *504*(7478), 84–88. https://doi.org/10.1038/nature12860

Stiger-Pouvreau, V., Mattio, L., De Ramon N'Yeurt, A., Uwai, S., Dominguez, H., Flórez-Fernández, N., Connan, S., & Critchley, A. T. (2023). A concise review of the highly diverse genus *Sargassum* C. Agardh with wide industrial potential. *Journal of Applied Phycology*, *35*(4), 1453–1483. https://doi.org/10.1007/s10811-023-02959-4

Tanniou, A., Vandanjon, L., Gonçalves, O., Kervarec, N., & Stiger-Pouvreau, V. (2015). Rapid geographical differentiation of the European spread brown macroalga *Sargassum muticum* using HRMAS NMR and Fourier-transform infrared spectroscopy. *Talanta*, *132*, 451–456. https://doi.org/10.1016/j.talanta.2014.09.002

Tsugawa, H., Ikeda, K., Takahashi, M., Satoh, A., Mori, Y., Uchino, H., Okahashi, N., Yamada, Y., Tada, I., Bonini, P., Higashi, Y., Okazaki, Y., Zhou, Z., Zhu, Z. J., Koelmel, J., Cajka, T., Fiehn, O., Saito, K., Arita, M., & Arita, M. (2020). A lipidome atlas in MS-DIAL 4. *Nature Biotechnology*, *38*(10), 1159–1163. https://doi.org/10.1038/s41587-020-0531-2

van Tussenbroek, B. I., Hernández Arana, H. A., Rodríguez-Martínez, R. E., Espinoza-Avalos, J., Canizales-Flores, H. M., González-Godoy, C. E., Barba-Santos, M. G., Vega-Zepeda, A., & Collado-Vides, L. (2017). Severe impacts of brown tides caused by *Sargassum* spp. on near-shore Caribbean seagrass communities. *Marine Pollution Bulletin*, *122*(1–2), 272–281. https://doi.org/10.1016/j.marpolbul.2017.06.057

van Tussenbroek, B. I., Monroy-Velázquez, L. V., Rodríguez, D., Suescún-Bolívar, L. P., Thomé, P. E., Cerqueda-García, D., García-Maldonado, J. Q., Martínez-López, I. G., López-Portillo, J. A., Barba-Santos, M. G., Gómez-Reali, M. A., & Escalante-Mancera, J. E. (2024). Monitoring drift and associated biodiversity of nearshore rafts of holopelagic *Sargassum* spp. in the Mexican Caribbean. *Aquatic Botany*, *195*, 103792. https://doi.org/10.1016/j.aquabot.2024.103792

Wang, M., Carver, J. J., Phelan, V. V., Sanchez, L. M., Garg, N., Peng, Y., Nguyen, D. D., Watrous, J., Kapono, C. A., Luzzatto-Knaan, T., Porto, C., Bouslimani, A., Melnik, A. V., Meehan, M. J., Liu, W. T., Crüsemann, M., Boudreau, P. D., Esquenazi, E., Sandoval-Calderón, M., … Bandeira, N. (2016). Sharing and community curation of mass spectrometry data with Global Natural Products Social Molecular Networking. *Nature Biotechnology*, *34*(8), 828–837. https://doi.org/10.1038/nbt.3597

Wang, M., Hu, C., Barnes, B. B., Mitchum, G., Lapointe, B., & Montoya, J. P. (2019). The great Atlantic *Sargassum* belt. *Science*, *365*(6448), 83–87.

Zianni, R., Bianco, G., Lelario, F., Losito, I., Palmisano, F., & Cataldi, T. R. I. (2013). Fatty acid neutral losses observed in tandem mass spectrometry with collision-induced dissociation allows regiochemical assignment of sulfoquinovosyl-diacylglycerols. *Journal of Mass Spectrometry*, *48*(2), 205–215. https://doi.org/10.1002/jms.3149

SUPPORTING INFORMATION

Additional supporting information can be found online in the Supporting Information section at the end of this article.

Figure S1. t-SNE molecular network representation constructed on MS^2 homology. The pie charts in the nodes represent abundance, and the colors correspond to the three morphotypes (red: SN8, blue: SN1, green: SF1 and gray: blank). Annotated metabolites identified from MS^2 standard database query clusters are boxed in black.

Figure S2. MS^2 spectrum of MGDG 16:0/16:4 (1).
Figure S3. MS^2 spectrum of MGDG 16:0/16:3 (2).
Figure S4. MS^2 spectrum of MGDG 16:0/16:2 (3).
Figure S5. MS^2 spectrum of MGDG 16:0/18:3 (4).
Figure S6. MS^2 spectrum of MGDG 16:0/18:2 (5).
Figure S7. MS^2 spectrum of MGDG 18:3/18:4 (6).
Figure S8. MS^2 spectrum of MGDG 18:3/18:3 (7).
Figure S9. MS^2 spectrum of DGDG 16:0/16:4 (8).
Figure S10. MS^2 spectrum of DGDG 16:0/16:3 (9).
Figure S11. MS^2 spectrum of DGDG 16:1/18:3 (10).
Figure S12. MS^2 spectrum of DGDG 16:0/18:3 (11).
Figure S13. MS^2 spectrum of SQDG 16:0/16:1 (12).
Figure S14. MS^2 spectrum of SQDG 16:0/16:0 (13).

Figure S15. MS^2 spectrum of SQDG 16:0/18:3 (14).
Figure S16. MS^2 spectrum of SQDG 16:0/18:1 (15).
Figure S17. Score plot of partial least squares discriminant analysis of ^1H NMR profiles of (a) acetone and (b) dichloromethane extracts from *Sargassum* morphotypes. PLS-DA loading plot of (c) acetone and (d) dichloromethane extracts.
Table S1. Major ions and their putative annotations and spectral matching information of compounds detected in pelagic *Sargassum* hydroethanolic extracts.

How to cite this article: Nirma, C., Stiger-Pouvreau, V., Levasseur, M., Touboul, D., Connan, S., & Petek, S. (2025). When chemistry meets taxonomy: Studying glycolipidic chemomarkers in pelagic *Sargassum* spp. (Phaeophyceae) using molecular networking. *Journal of Phycology*, *00*, 1–14. https://doi.org/10.1111/jpy.70116